

THE DARK MATTER DENSITY PROFILE OF THE LENSING CLUSTER MS2137-23: A TEST OF THE COLD DARK MATTER PARADIGM¹

DAVID J. SAND

California Institute of Technology, Physics, mailcode 103–33, Pasadena, CA 91125

TOMMASO TREU & RICHARD S. ELLIS

California Institute of Technology, Astronomy, mailcode 105–24, Pasadena, CA 91125

ApJ Letters, in press

ABSTRACT

We present new spectroscopic observations of the gravitational arcs and the brightest cluster galaxy (BCG) in the cluster MS2137-23 ($z = 0.313$) obtained with the Echelle Spectrograph and Imager on the Keck II telescope. We find that the tangential and radial arcs arise from sources at almost identical redshifts ($z = 1.501, 1.502$). We combine the measured stellar velocity dispersion profile of the BCG with a lensing analysis to constrain the distribution of dark and stellar matter in the central 100 kpc of the cluster. Our data indicate a remarkably flat inner slope for the dark matter profile, $\rho_d \propto r^{-\beta}$, with $\beta < 0.9$ at 99% CL. Steep inner slopes obtained in cold dark matter cosmological simulations – such as Navarro Frenk & White ($\beta = 1$) or Moore (1.5) universal dark matter profiles – are ruled out at better than 99%CL. As baryon collapse is likely to have steepened the dark matter profile from its original form, our data provides a powerful test of the cold dark matter paradigm at the cluster mass scale.

Subject headings: gravitational lensing — galaxies: elliptical and lenticular, cD — galaxies: evolution — galaxies: formation — galaxies: structure

1. INTRODUCTION

A fundamental result arising from cold dark matter (CDM) numerical simulations is that the density profiles of DM halos are universal in form across a wide range of mass scales from dwarf galaxies to clusters of galaxies (Navarro, Frenk & White 1997, hereafter NFW). Internal to some scale radius r_{sc} , the dark matter profile assumes a power law form, $\rho_d \propto r^{-\beta}$. Whilst there is some dispute amongst the simulators about the precise value of β with values ranging from 1.0 to 1.5, (Moore et al. 1998, hereafter M98; Ghigna et al. 2000, Power et al. 2002), a clear measurement of β in a range of objects would offer a powerful test of the CDM paradigm.

The largest observational effort in this respect to date has been via dynamical studies of low surface brightness (LSB) and dwarf galaxies, suggesting softer ($\beta < 1$) DM cores than expected on the basis of the numerical simulations (e.g. de Blok & Bosma 2002, Salucci & Burkert 2000), although the issue remains somewhat controversial (e.g. van den Bosch & Swaters 2001). Similar tests have recently been extended to regular spiral (Jimenez, Verde & Oh 2002) and elliptical galaxies (Treu & Koopmans 2002). Some observational constraints are available at the scale of massive clusters, from lensing (e.g. Tyson, Kochanski & Dell’Antonio 1998; Williams et al. 1999; Smith et al. 2001), X-ray analysis (Mahdavi & Geller 2001) and dynamics of cD galaxies (Kelson et al. 2002). Since massive clusters probe a totally different scale and physical conditions than galaxies, it is crucial to understand their mass distribution to test the universality of the DM profiles.

In this paper we present the first application of a new method to determine the luminous and dark mass distribution in the inner regions of massive clusters with giant

arcs around a central BCG. The method combines lensing analysis with stellar kinematical measurements of the BCG. The two ingredients provide complementary information on the relevant scales (~ 100 kpc), allowing us to disentangle the luminous and dark components of the total mass distribution.

We have chosen the cluster MS2137-23 as a first application of our method since it is an approximately round system, has an isolated BCG and a very well-studied arc system. Fort et al. (1992) first pointed out the potential significance of the radial and tangential gravitational arcs as a means of constraining the mass distribution on $\simeq 100$ kpc scales, and mass models have been developed subsequently (Mellier et al. 1993, Hammer et al. 1997; hereafter M93, H97). The redshifts of the radial and tangential arcs were predicted to lie in the range $1 < z < 2$ (M93). A key issue in the earlier work is whether the radial arc is, in fact, a lensed feature. M93 and Miralde-Escudé (1995; hereafter ME95) also point out the importance of determining the stellar velocity dispersion profile of the BCG to weigh the stellar contribution to the mass.

Following the earlier suggestions, we present new observations of the cluster MS2137-23 with the Keck II telescope. We provide spectroscopic confirmation of the arcs and measure a velocity dispersion profile for the central BCG. The spectroscopic data are used together with archival HST images to constrain the luminous and DM distribution of the cluster. In the following, r is the radial coordinate in 3-D space, while R is the radial coordinate in 2-D projected space. We adopt $H_0 = 65 \text{ km s}^{-1} \text{ Mpc}^{-1}$, $\Omega_m = 0.3$ and $\Omega_\Lambda = 0.7$ for the cosmological parameters.

¹ Based on observations collected at the Keck Observatory, which is operated jointly by the California Institute of Technology and the University of California, and with the NASA/ESA HST, obtained at STScI, which is operated by AURA, under NASA contract NAS5-26555.

2. OBSERVATIONS

2.1. *Keck Spectroscopy*

We observed MS2137-23 using the Echelle Spectrograph and Imager (ESI; Sheinis et al. 2002) on the W. M. Keck-II telescope for a total integration time of 4900s ($2 \times 1800\text{s} + 1300\text{s}$) on 21 July, 2001. The seeing was $0''.6$ and the $1''.25 \times 20''$ slit was oriented North-South to include the BCG, radial arc, and tangential arc (Figure 1). The spectroscopic goals were two-fold: a determination of the redshift of the arcs and a measurement of the internal kinematics of the central galaxy. An IRAF package was developed for the specific task of removing echelle distortions while preserving the 2-D shape of the spectrum essential for the latter goal (EASI2D, Sand et al. 2002, in preparation). The instrumental resolution of ESI was measured from unblended sky lines to be $30 \pm 7 \text{ km s}^{-1}$.

The velocity dispersion profile of the BCG (Figure 2) was measured using spectral templates based on several G-K giants observed with a $0''.3$ slit. These were smoothed to match the instrumental resolution of the $1''.25$ slit and redshifted to that of the BCG ($z=0.313$). Analysis was restricted to a region around the G band by virtue of the high signal/noise and minimal effect of sky line residuals, using the Gauss-Hermite pixel-fitting software (van der Marel 1994). The error bars shown in Fig. 2 represent a combination of uncertainties arising from Poisson noise and systematics, the latter determined from the scatter observed using different templates and continuum fits.

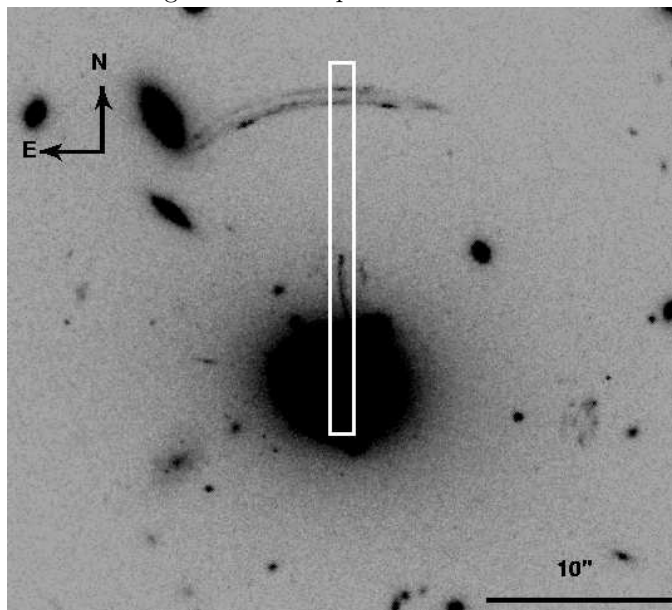


FIG. 1.— HST F702W image of MS2137-23. The rectangular box shows the dimensions ($1''.25 \times 20''$) and position of the ESI slit used to make the observations. The BCG, the radial and tangential arc are clearly visible at the bottom, center, and upper end of the slit.

The high spectral resolution of ESI proved crucial in clinching the redshifts of the arcs as the emission lines are located in a crowded region of OH sky background. The two top panels in Fig. 2 show the relevant portion of the ESI spectra for the tangential and radial arcs, with the observed emission lines identified as the [OII] doublet at $z = 1.501$ and $z = 1.502$ respectively. The [OII] doublet is clearly resolved for the tangential arc and it is reasonable to suppose that the missing component for the radial arc is

obscured by sky emission. No other lines are detected on either spectra, down to the blue cutoff of ESI at $\sim 3900\text{\AA}$. This makes it unlikely that the single line observed for the radial arc is any of the common lines such as $\text{H}\alpha$, $\text{H}\beta$, [OIII]4959, 5007, CIV1549, HeII1640, C[III]1909 because bluer lines would be detected assuming typical flux ratios. The identification of the line with $\text{Ly}\alpha$ at $z = 6.66$ is also unlikely given that the arc is detected in the HST F702W image (see below). Detailed modeling of MS2137-23 based on the image configurations predicted that the sources for the arcs would be at nearly the same redshift (M93, H97).

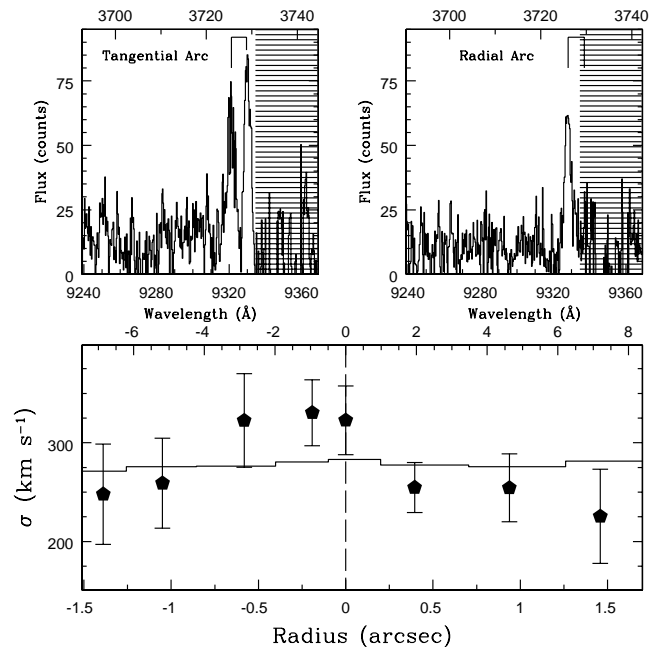


FIG. 2.— Spectroscopic results: (Top) Strong emission lines detected in the spectra of the tangential and radial arcs. These are identified as [OII]3726,3729 at $z = 1.501$ and $z = 1.502$ respectively (marked). It is argued that the missing 3729Å line in the radial arc is obscured by sky emission. (Bottom) Stellar velocity dispersion profile of the brightest cluster galaxy (points with error bars). The superimposed histogram shows the profile of the best fitting Jaffe + generalized NFW mass model (see Sec. 3 for details), taking into account the effects of seeing ($0''.6$), slit width, and radial binning.

2.2. *Hubble Space Telescope Imaging*

HST WFPC2 images of MS2137-23 (GO 5402, PI: Gioia), comprising 10 F702W exposures with a total integration time of 22.2ks, were used to measure the surface photometry of the BCG and to locate arc positions. The exposures were reduced in a standard way, using the IRAF package DRIZZLE (Fruchter & Hook 2002).

The circularized surface brightness profile (in agreement with H97) was obtained using the IRAF task ELLIPSE and a fit performed as described in Treu et al. (1998, 2001a) taking into account the HST point-spread function. The best fitting $R^{1/4}$ parameters are summarized in Table 1. To convert from F702W magnitudes to V magnitudes a k-color correction was calculated using the same method as Treu et al. (1999). Rest frame photometric quantities were corrected for Galactic extinction using $A_{F702W} = 2.435E(B-V) = 0.122$ (Schlegel et al. 1998).

| | |
|---|----------------------|
| Redshift (BCG) | 0.313 ± 0.001 |
| Radial critical line | $4''.5 \pm 0''.3$ |
| Tangential critical line | $15''.35 \pm 0''.20$ |
| $(1-b/a)_e$ | 0.17 ± 0.01 |
| F702W (mag) | 16.48 ± 0.07 |
| $SB_{e,F702W}$ (mag/arcsec ²) | 23.58 ± 0.34 |
| $R_{e,F702W}$ | $5''.02 \pm 0''.50$ |
| M_V (mag) | -24.38 ± 0.09 |
| $SB_{e,V}$ (mag/arcsec ²) | 22.76 ± 0.34 |
| $R_{e,V}$ (kpc) | 24.80 ± 1.68 |

TABLE 1: Relevant spectro-photometric quantities

3. LUMINOUS AND DARK MATTER DISTRIBUTION

We now combine the observed spectroscopic and photometric data to constrain the matter distribution in the central region of MS2137-23. First we introduce a simple two-component spherical mass model comprising the stellar mass of the BCG and a DM halo (Sec. 3.1). We then constrain the free parameters of the model using the position of the critical lines (3.2) and the velocity dispersion profile (3.3).

3.1. Mass model

For the luminous component we used a Jaffe (1983)

$$\rho_L(r) = \frac{M_L r_J}{4\pi r^2 (r_J + r)^2}, \quad (1)$$

mass density profile of total mass M_L , which reproduces well¹ the observed surface brightness profile (with $R_e = 0.76r_J$). The DM halo is modeled as,

$$\rho_d(r) = \frac{\rho_c \delta_c}{(r/r_{sc})^\beta (1 + (r/r_{sc}))^{3-\beta}}, \quad (2)$$

representing a generalization of the CDM-motivated halos, with an inner slope β (NFW and M98 correspond to $\beta = 1, 1.5$ respectively; ρ_c is the critical density). We assume that the BCG lies at the center of the overall potential.

For a given stellar mass-to-light ratio M_*/L_V both M_L and r_J can be deduced from the surface photometry leaving 4 free parameters in our mass model: 1) M_*/L_V ; 2) the inner slope of the DM profile β ; 3) the DM density scale δ_c ; and 4) the DM scale radius r_{sc} .

3.2. Gravitational Lensing

Given our two-component spherical model, we adopted a simple lensing analysis using only the positions and redshifts of the radial and tangential arcs (see Bartelmann 1996).

The locations of the radial and tangential arcs can be estimated by calculating the position of the corresponding radial and tangential critical curves of the projected mass distribution. The Jacobian matrix of the lens mapping has two eigenvalues, $\lambda_r = 1 - \frac{d}{dx} \frac{m}{x}$ and $\lambda_t = 1 - \frac{m}{x^2}$, where $x = R/r_{sc}$ and m is a dimensionless function proportional to the mass inside projected dimensionless radius x (see, e. g., Bartelmann 1996, Schneider, Ehlers, Falco 1992).

¹ As a check of the results, we also considered a Hernquist (1990) luminous mass distribution. The results on β (see below) are virtually unchanged, while slightly larger values of M/L for the stellar component are obtained.

² Spherical dynamical models have been shown to reproduce accurately the kinematics of slightly elongated galaxies like the BCG (e.g. Kronawitter et al. 2000).

Tangential and radial critical curves occur when $\lambda_t = 0$ and $\lambda_r = 0$, respectively. In practice, the position of the tangential arc constrains the *total enclosed mass*, while the position of the radial arc constrains its *derivative*. A proper account of ellipticity is essential for detailed lens modeling where the shape, magnification, and morphology of multiple lensed images is being reproduced. ME95, however, considered several different simple mass models where only the position of the radial and tangential critical lines were being measured and found that the position of the two was affected very little by the introduction of ellipticity. Therefore, we conclude that a spherical model is appropriate for our analysis.

For every set of free parameters $\{M_*/L_V, \beta, \delta_c, r_{sc}\}$, we can compute the predicted position of the arcs, find the likelihood assuming gaussian distributions, and constrain the acceptable mass models. The largest radius at which the mass is probed is that corresponding to the location of the tangential arc (75.8 kpc). Now r_{sc} is expected to be much greater than 100 kpc in CDM clusters (Bullock et al. 2001; see also Wu 2000). In this case, the location of the critical lines depends only marginally on r_{sc} and the combined luminous and dark density profile has only 3 free parameters (we fix $r_{sc} = 400$ kpc in the following). Fig. 3 shows the likelihood contours (68%, 95% and 99%) in β vs. M_*/L_V space, obtained using the likelihood ratio statistic after marginalization with respect to δ_c . Note that with lensing alone we can rule out with greater than 95% confidence a M98 DM density profile ($\beta=1.5$).

3.3. Lensing + Dynamics

The full power of our analysis is only realized when we combine the earlier constraints with those made by measuring the spatially-resolved stellar velocity dispersion profile of the BCG. Given our two-component mass model (Section 3.1), we solved the spherical Jeans equation (e.g. Binney & Tremaine 1987) assuming an isotropic velocity ellipsoid for the luminous component.²

The assumption of isotropy in the region probed (within 30 % of R_e) we justify both on theoretical and observational grounds. Numerical simulations (e. g. van Albada 1982) and observations (e.g. Gerhard et al. 2001; Koopmans & Treu 2002) appear to rule out significant tangential anisotropy and permitting some radial anisotropy only at large radii. Strong radial anisotropy in the very central regions can also be ruled out based on the grounds of stability (e. g. Merritt & Aguilar 1985; Stiavelli & Sparke 1991) and consistency requirements (Ciotti 1999). However, as a check, we ran Osipkov-Merritt (Osipkov 1979; Merritt 1985a,b) models with anisotropy radius set equal to progressively lower radii. Moving the anisotropy radius towards zero pushes the likelihood contours towards lower values of β .

For each set of parameters in the lens model, we computed the likelihood given the velocity dispersion profile, taking into account the effects of seeing, radial binning, and finite slit width. The total likelihood was computed by multiplying the velocity dispersion likelihood by the

likelihood obtained with the lensing analysis. The bottom panel in Fig. 3 shows the final results of the combined analysis. With 99% confidence, M_*/L_V lies between 2.3 and 3.7 (broadly consistent with local values after passive evolution), with the inner DM slope (β) lying between 0.05 and 0.8, flatter than that expected from CDM simulations. The best-fitting parameters are $M_*/L_V = 3.1 M_\odot/L_{\odot,V}$, $\beta = 0.35$, $\delta_c = 24000$.

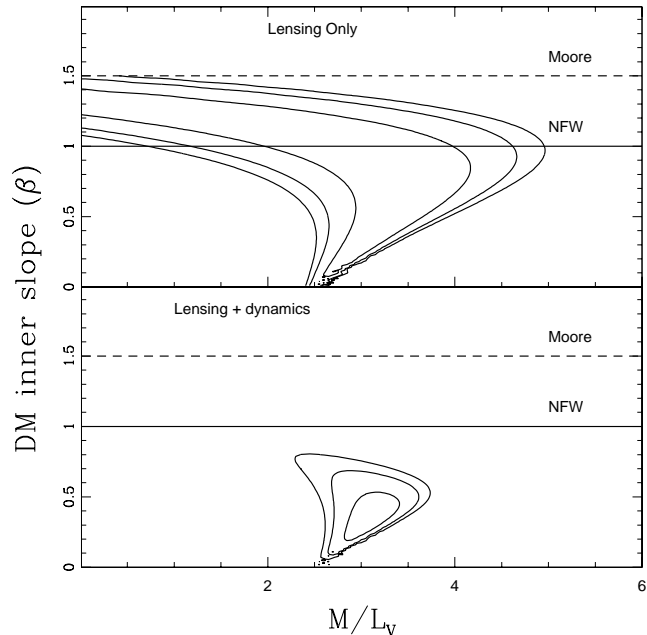


FIG. 3.— Likelihood contours (68%, 95%, and 99%) obtained for the mass modeling of MS2137-23 with a Jaffe luminous distribution plus a generalized NFW DM distribution. (Top): Contours obtained from the position of the radial and tangential arcs alone. Note that a M98 ($\beta = 1.5$) profile is excluded at the 95% level. (Bottom): Contours obtained including the measured velocity dispersion profile. Note the improved constraints on the mass parameters and that NFW profiles are clearly ruled out at the 99% level.

To check our results, we changed R_e by 10% with a negligible effect on the likelihood contours. Similarly, the contours are virtually unchanged by offsets of $0''.5$ in the position of the tangential arc and by changing the seeing by 30%. Changing the position of the radial critical line by $\pm 0''.5$ shifts the likelihood contours by ± 0.1 in the β direction.

Systematic offsets of the velocity dispersion profile due to template mismatch and poor continuum fitting introduce correlation between the kinematic points that are not considered in the likelihood ratio analysis. To investigate this, we have repeated the analysis with the velocity dispersion profile shifted by the estimated systematic error ($\sim 15 \text{ km s}^{-1}$). A lower overall velocity dispersion profiles shifts our likelihood contours towards lower β ($\beta < 0.65$ 99 % CL), and viceversa ($\beta < 0.9$ 99 % CL): our hard 99%

CL upper limit is $\beta < 0.9$.

4. SUMMARY AND DISCUSSION

We have secured spectroscopic redshifts for the radial and tangential arcs in the cluster MS 2137-23 and determined the velocity dispersion profile of the BCG to a physical radius of $\simeq 8$ kpc. We have combined these measurements with the lensing geometry in order to construct a self-consistent model of the mass distribution in the cluster core. Using a spherically symmetric luminous and DM mass distribution, we rule out the presence of a DM halo with an inner slope $\beta > 0.9$ at greater than 99% confidence, including systematics. M98 and NFW-type halos with $\beta \geq 1.0$ are inconsistent with the mass distribution in the core of MS2137-23.

Since the infall of baryons associated with the BCG are likely to *steepen* the DM halo (Blumenthal et al 1986; Mo, Mao and White 1998), our measured profile may imply the original DM profile was even flatter. A full modeling of this process is beyond the scope of this letter, but this strengthens our conclusion that the inner regions of the DM halo of MS2137-23 cannot be described by CDM-motivated universal halos. A potential concern is that our models have only two mass components, but X-ray emitting gas could be a non-negligible third massive component. Using ROSAT observations of MS2137-23 (Ettori & Fabian 1999) we estimate that removing the X-ray component will steepen the resulting DM halo slope by less than $\simeq 0.1$ and therefore does not change dramatically the result.

Finally, individual halo shapes can depart from the ensemble average behavior. Therefore it is necessary to apply such a test to a sample of clusters. Our simple method is applicable to all approximately round clusters with a massive galaxy at their center, provided that they have at least a giant tangential arc (radial arcs further enhance the sensitivity but are not required). We are in the process of collecting data for a dozen clusters with the aim of performing such a statistical test.

We are grateful to A. Benson, J.-P. Kneib, L. Koopmans for insightful discussions and comments on this project, and to P. Shopbell for numerous computer tips. We acknowledge the use of the Gauss-Hermite Pixel Fitting Software developed by R. P. van der Marel. We acknowledge financial support for proposal number HST-AR-09527 provided by NASA through a grant from STScI, which is operated by AURA, under NASA contract NAS5-26555. Finally, the authors wish to recognize and acknowledge the cultural role and reverence that the summit of Mauna Kea has always had within the indigenous Hawaiian community. We are most fortunate to have the opportunity to conduct observations from this mountain.

REFERENCES

- Bartelmann, M. 1996, A&A, 313, 697
 Binney, J., & Tremaine, S. 1987, Galactic Dynamics, Princeton University Press, Princeton
 Blumenthal, G. R., Faber, S. M., Flores, R., & Primack, J. R. 1986, ApJ, 301, 27
 Bullock, J. S., Kolatt T. S., Sigad, Y., Somerville, R. S., Kravtsov, A. V., Klypin, A. A., Primack, J. R., & Dekel, A. 2001, MNRAS, 321, 598
 Ciotti, L. 1999, ApJ, 520, 574
 de Blok, W. J. G., & Bosma, A. 2002, A&A, 385, 816
 Ettori, S., & Fabian A. C. 2002, MNRAS, 305, 834

- Fort, B., Le Fevre, O., Hammer, F., & Cailloux, M. 1992, *ApJ*, 399, L125
- Fruchter, A. S., & Hook, R. N. 2002, *PASP*, 114, 14
- Gerhard, O., Kronawitter, A., Saglia, R. P., & Bender, R. 2001, *AJ*, 121, 1936
- Ghigna, S., Moore, B., Governato, F., Lake, G., Quinn, T., & Stadel, J. 2000, *ApJ*, 544, 616
- Hammer, F., Gioia, I., Shaya, E., Teyssandier, P., Le Fevre, O., & Luppino, G. 1997, *ApJ*, 491, 477
- Hernquist, L. 1990, *ApJ*, 356, 359
- Jaffe, W. 1983, *MNRAS*, 202, 995
- Jimenez, R., Verde, L., & Oh, S. P. 2002, *MNRAS*, submitted (astro-ph/0201352)
- Kelson, D., Zabludoff, A., Williams, K., Trager, S., Mulchaey, J., & Bolte, M. 2002, *ApJ*, accepted (astro-ph/0205316)
- Koopmans, L. V. E., & Treu, T. 2002, *ApJ*, submitted, astro-ph/0205335
- Kronawitter, A., Saglia, R.P., Gerhard, O., & Bender, R. 2000, *A&AS*, 144, 53
- Mahdavi, A., & Geller, M. 2001, *AAS, Mtg.* 199, 142.04
- Mellier, Y., Fort, B., & Kneib, J. 1993, *ApJ*, 407, 33
- Merritt, D. 1985a, *AJ*, 90, 1027
- Merritt, D. 1985b, *MNRAS*, 214, 25
- Merritt, D., & Aguilar, L. A. 1985, *MNRAS*, 217, 787
- Miralde-Escudé, J. 1995, *ApJ*, 438, 514
- Mo, H., Mao, S., & White S. D. M. 1998, *MNRAS*, 297, 71
- Moore, B., Governato, F., Quinn, T., Stadel, J. & Lake, G. 1998, *ApJ*, 499, L5
- Navarro, J., Frenk, C. S., & White S. D. M. 1997, *ApJ*, 490, 493
- Osipkov, L. P. 1979, *Pis'ma Astron. Zh.*, 5, 77
- Power, C., Navarro, J., Jenkins, A., Frenk, C., White, S., Springel, V., Stadel, J., & Quinn, T. 2002, *MNRAS*, submitted (astro-ph/0201544)
- Salucci, P., & Burkert, A. 2000, *ApJ*, 537, L9
- Schneider, P., Ehlers, J. & Falco, E. E. 1992, *Gravitational Lenses*, Springer-Verlag, Berlin.
- Schlegel, D. J., Finkbeiner, D. P., & Davis, M. 2000, *ApJ*, 500, 525
- Sheinis, A. I., et al. 2002, *PASP*, in press, astro-ph/0204297
- Smith, G. P., Kneib, J.-P., Ebeling, H., Czoske, O., & Smail, I. R. 2001, *ApJ*, 552, 493
- Stiavelli, M., & Sparke, L. 1991, *ApJ*, 382, 466
- Treu, T., & Koopmans, L. V. E. 2002, *ApJ*, 575, in press
- Treu, T., Stiavelli, M., Bertin G., Casertano, C., & Møller, P. 2001, *MNRAS*, 326, 237
- Treu, T., Stiavelli, M., Casertano, C., Møller, P., & Bertin G. 1999, *MNRAS*, 308, 1307
- Treu, T., Stiavelli, M., Casertano, C., Møller, P., & Bertin, G. 2002, *ApJ*, 564, L13
- Tyson, A., Kochanski, G., & dell'Antonio, I., 1998, *ApJ*, 498, L107
- van Albada, T.S. 1982, *MNRAS*, 201, 939
- van den Bosch, F. C. & Swaters, R. A. 2001, *MNRAS*, 325, 1017
- van der Marel, R. P. 1994, *MNRAS*, 270, 271
- Williams, L., Navarro, J., & Bartelmann, M. 1999, *ApJ*, 527, 535
- Wu, X. 2000, *MNRAS*, 316, 299